

# AeroHaptix: A Wearable Vibrotactile Feedback System for Enhancing Collision Avoidance in UAV Teleoperation

Bingjian Huang, Zhecheng Wang, Qilong Cheng, Siyi Ren, Hanfeng Cai, Antonio Alvarez Valdivia, Karthik Mahadevan, and Daniel Wigdor

**Abstract**—Haptic feedback enhances collision avoidance by providing directional obstacle information to operators during unmanned aerial vehicle (UAV) teleoperation. However, such feedback is often rendered via haptic joysticks, which are unfamiliar to UAV operators and limited to single direction force feedback. Additionally, the direct coupling between the input device and the feedback method diminishes an operators’ sense of control and causes oscillatory movements. To overcome these limitations, we propose AeroHaptix, a wearable haptic feedback system that uses spatial vibrations to communicate multiple obstacle directions to operators simultaneously, without interfering the input control. The layout of vibrotactile actuators was determined via a perceptual study to eliminate perceptual biases and achieve uniform spatial coverage. A novel rendering algorithm, MultiCBF, extends control barrier functions to support multi-directional feedback. Our system evaluation showed that compared to the baseline condition, AeroHaptix effectively reduced the number of collisions and input disagreement. Additionally, operators reported that AeroHaptix was more helpful than the force feedback method, with comparable workload and situational awareness.

## I. INTRODUCTION

Unmanned aerial vehicle (UAV) teleoperation enables operators to pilot UAVs beyond their visual line of sight, enabling for tasks to be completed in situations that are either difficult or dangerous for humans to be present. Teleoperation is challenging, however, because the operator is physically separated from the UAV, which limits an operator’s ability to perceive obstacles and avoid collisions. Recent UAV teleoperation systems have utilized haptic feedback to deliver obstacle information so that operators can safely steer UAVs. To translate obstacle information into haptic feedback, prior work has developed collision avoidance algorithms such as parametric risk fields [1], time-to-impact [2], dynamic kinesthetic boundary [3], and control barrier functions (CBF) [4].

Despite the advancement of collision avoidance algorithms, the devices used to render haptic feedback are primarily commercial haptic joysticks with three degree-of-freedom (DoF) force feedback [5]–[7]. Although these devices have proven useful in collision avoidance tasks [8], [9], they are rarely adopted in real-world UAV operations due to the high transition cost from standard radio control (RC) controllers to such unfamiliar devices. The use of such devices is further constrained to indoor environments as haptic joysticks must be mounted to an immovable surface to provide accurate force feedback. Furthermore, the limited information bandwidth of haptic joysticks restricts force feedback to being rendered in one direction [4], [10], thus compromising situational awareness in environments

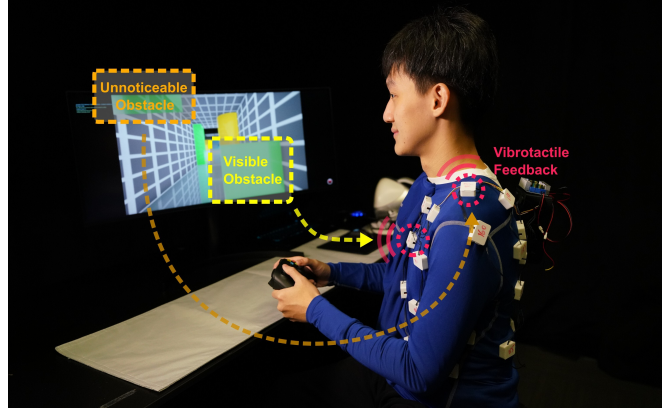


Fig. 1: AeroHaptix assists UAV operators with collision avoidance by delivering spatial vibrotactile feedback on the body about multiple obstacle directions. Operators can not only see and feel visible obstacles (yellow), but also perceive obstacles out of view (orange).

with multiple obstacles. Since haptic joysticks exert force feedback on the hand, the direct coupling of input and output channels impairs UAV control precision, leading to oscillatory behavior in cluttered environments [9] and low user acceptance [11]. Alternative devices such as cable-driven exoskeletons [12], [13] solved the mobility issue, but added new challenges such as physical fatigue and limited degrees of freedom.

To address these limitations, we designed a wearable haptic feedback system, AeroHaptix, that renders vibrotactile feedback at thirty-two upper body positions to deliver obstacle directions. Since the feedback is provided as vibration cues on the body, it does not hinder hand movement and can be seamlessly integrated into existing teleoperation control workflows (e.g., using RC controllers). We conducted a perceptual study with ten participants to collect data on the mapping between body positions and spatial directions, and employed a neural network to generate the layout of vibrotactile actuators on the body. We also designed MultiCBF, a novel collision avoidance algorithm that extends previous CBF methods to render multi-directional haptic feedback. Our system evaluation showed that compared to the baseline condition, AeroHaptix effectively reduced the number of collisions and input disagreement. Additionally, operators reported that AeroHaptix was more helpful than the force feedback method, with comparable workload and situational awareness.

## II. RELATED WORK

Of most relevance to the present research is prior literature on (a) collision avoidance algorithms for UAV teleoperation and (b) vibrotactile feedback to convey spatial information.

### A. Collision Avoidance Algorithms

Collision avoidance algorithms were first utilized for unmanned ground vehicle teleoperation. In 1998, Hong et al. proposed an artificial force field algorithm to generate artificial forces based on the potential fields of vehicle and obstacles [14]. This concept was later adopted for UAVs by Boschloo et al. [15] and Lam et al. [1], who developed basic risk field and parametric risk field algorithms respectively. These methods successfully reduced collisions but faced difficulties when users navigated through narrow spaces. To further improve operation, Brandt and Colton introduced time-to-impact and virtual string algorithms that calculated the virtual impact forces between a UAV and obstacles [2]. While these algorithms further reduced collisions and workloads, the force feedback they generated was found to cause UAVs to oscillate in cluttered environments [9].

Alternatively, other researchers have proposed algorithms that override user input with safer values, such as dynamic kinesthetic boundary [3], [16] and obstacle avoidance system for teleoperation [17]. While these algorithms eliminated collisions, they reduced operators' sense of control and user acceptance. More recently, Zhang et al. applied control barrier functions (CBF) to UAV teleoperation [4], which modify an input control signal to closely match the original while adhering to safety constraints. They also designed a haptic shared autonomy control scheme that enhanced operators' sense of control [8]. We extended their CBF algorithm to support multi-point haptic feedback and thus the simultaneous representation of multiple obstacles.

### B. Vibrotactile Feedback to Convey Spatial Information

Vibrotactile feedback conveys sensory information to humans via actuators vibrating on the skin. Prior work has demonstrated the application of vibrotactile feedback in various domains where spatial information is crucial. For example, vibrotactile headbands have been used to assist users in locating 3D objects and improving spatial awareness in virtual reality [18], [19]. Vibrotactile actuators have also been placed on the body to enhance obstacle detection and navigation for blind and visually-impaired people [20]–[22]. Within robotics, vibrations have been used to communicate handover positions and predicted trajectories of robotic arms [23], [24], hydrodynamic flow near underwater robots [25], and obstacle positions around UGVs [26]. These examples reaffirm the applicability of using vibrotactile feedback to convey spatial information.

Compared to previous applications, delivering obstacle directions during UAV teleoperation is more challenging, because it requires numerous actuators placed in a custom layout on the body to precisely represent obstacle directions. Current vibrotactile systems such as TactJam [27] and VHP [28] offer great customizability but only support up to

12 actuators. In contrast, solutions like bHaptics X40 [29]) support numerous actuators but have predetermined positions on the body and limited body coverage. Therefore, we developed custom hardware for AeroHaptix that overcame the above challenges.

## III. AEROHAPTIX HARDWARE DESIGN

To support UAV teleoperation tasks, AeroHaptix was designed to support numerous actuators, customized layouts, and low-latency control. Its design had three requirements:

- **R1:** support the fine-grained control of a large number of actuators to distinguish obstacles from different directions;
- **R2:** support the reconfiguration of actuator layouts so actuators could be freely adjusted as needed; and
- **R3:** support low-latency communication so multi-point feedback could be activated without a noticeable delay.

AeroHaptix had a central unit and multiple chains of vibration units (Figure 2). Each vibration unit consisted of a voice coil actuator (PUI Audio, Model# = HD-VA3222), a custom-designed PCB board, and 3D-printed parts. The actuator was 32 mm by 22 mm, with frequency responses from 80 - 500 Hz. When driven by 133 Hz 1.5  $V_{rms}$  signal, it had a maximum acceleration of 2.52 Gp-p. The PCB included a PIC16F18313 Microcontroller Unit (MCU) and a DRV8837 H-bridge motor driver. The MCU received and transmitted UART commands and generated waveforms. When the MCU received a *start* signal, it sent a waveform to the H-bridge to activate the actuator. The MCU had fine-grained control (**R1**) over 16 intensity levels, 4 frequencies, and two waveforms. The 3D-printed parts included a cap and an enclosure that ensured components' stability during vibrations, and a bottom ring that enabled easy repositioning on garment (**R2**) via press-fit.

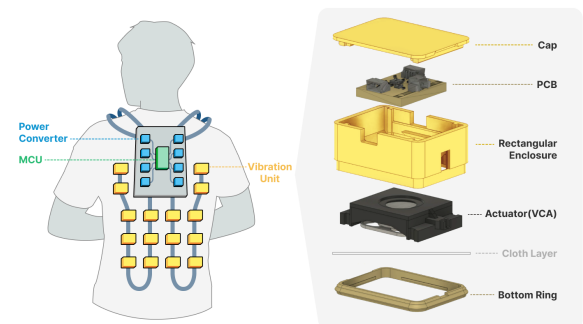


Fig. 2: Aerohaptix's hardware design, with an exploded view of a vibration unit.

To support low-latency communication (**R3**), we designed a chain-connection topology and a high-speed UART protocol (Figure 3). Each chain had a central unit, a power converter, and a maximum of 20 vibration units. Each vibration unit received a UART command from the previous unit and determined whether to execute it or propagate it to the next unit. The UART protocol transmitted two-byte messages at a baud rate of 115.2 kHz with parity check

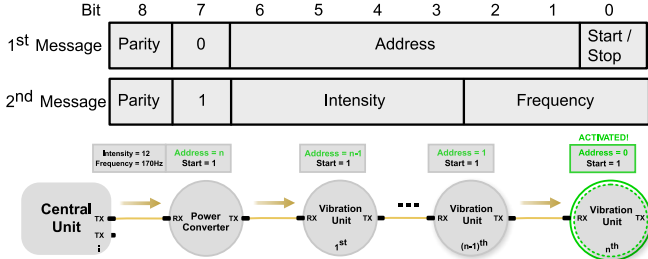


Fig. 3: The data transmission on each chain used a two-byte UART protocol. The central unit sent a command with address  $n$ , and each unit deducted the address by 1 until it reached the target unit.

bits. The first byte contained the target unit address and a *start/stop* toggle bit. The second byte contained vibration parameters for the target unit (i.e., intensity and frequency). A technical evaluation demonstrated that there was a  $125\ \mu\text{s}$  delay between two vibration units. With 20 units, the total delay was only 2.5 ms, fulfilling the requirement.

#### IV. HAPTIC ACTUATOR LAYOUT OPTIMIZATION

To achieve comprehensive coverage of obstacle directions (**R1**), one naive approach is to uniformly distribute actuators around the body. However, previous research has shown that due to proprioceptive biases, a uniform actuator layout on the waist could lead to uneven coverage of 2D directions on the azimuth plane [30]. Therefore, we designed a perceptual study to collect data about position-direction mappings on the upper body. Then, we trained a neural network to generate an optimized actuator layout.

Ten participants (6 male, 4 female; mean age = 25 years, std = 2 years) were recruited for the study. Each study lasted 40 minutes and each participant received \$20 CAD as compensation. The study was approved by our university's Research Ethics Board.

##### A. Data Collection Procedure

The initial layout used during the study was a 46-actuator grid that was uniformly distributed on the upper body (i.e., red dots in Figure 5). Each actuator was positioned equidistantly from its neighbors, with 18 actuators on the front and back, 3 on each side of the waist, and 2 on each shoulder. Following VibroMap [31], the inter-actuator distances were about 8 cm.

A Unity 3D virtual reality application was developed for the study. Participants wore a Meta Quest 2 headset and stood in a virtual space with coordinates surrounding them (Figure 4). They received a vibrotactile cue from an individual actuator and used an extended ray emitted from a Quest 2 controller to point in the perceived direction of the actuator. They then clicked the trigger button on the controller to confirm their perceived direction. Each participant completed 230 trials in a randomized order (i.e., 46 actuators  $\times$  5 repetitions).

##### B. Layout Optimization

We collected 2,300 mappings between an actuator positions on participants' body surfaces  $p \in \Omega \subset \mathbb{R}^3$  and

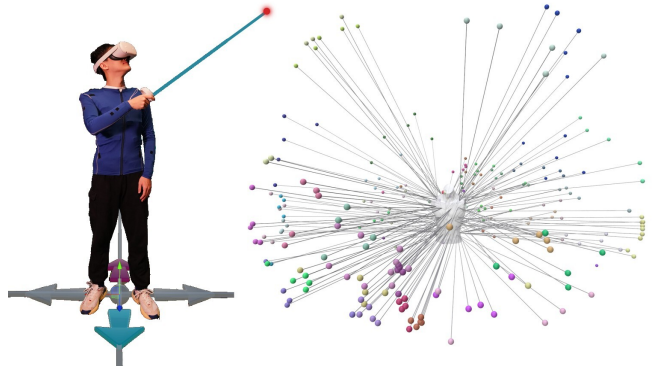


Fig. 4: Left: An illustration of the virtual reality study environment where a user is pointing in the direction of the vibrotactile cue they perceived on their body. Right: Example data points collected from one participant, where points of the same color were from the same actuator.

the obstacle directions participants perceived  $(\vartheta, \varphi)$  on a 2-sphere  $S^2$ , parameterized by a polar angle  $\vartheta$  and an azimuth angle  $\varphi$ . This data was used to approximate an inverse mapping from  $S^2$  to  $\Omega \subset \mathbb{R}^3$  using a Multi-layer Perceptron neural network:

$$f_\theta = \arg \min_{\theta} \sum_{i=1}^N \|f_\theta(\vartheta, \varphi) - p\|^2 + \lambda \sum_{i=1}^N |\nabla f_\theta(\vartheta, \varphi)|, \quad (1)$$

where  $\theta$  represented the neural network parameters and  $\lambda$  was the regularization term weight. The network featured five 64-unit hidden layers with ReLU activation. To promote mapping smoothness, we incorporated a total variation regularization term into the mean squared error loss function.

##### C. Final Layout

Previous studies have found that humans can discriminate force feedback directions on the hand with  $30^\circ$  resolutions [32], [33]. To achieve similar discriminability with vibrations on the body, we uniformly sampled 32 directions  $\phi = (\vartheta, \varphi)$  in 3D space  $S^2$ , where  $\vartheta \in \{\frac{\pi}{6}, \frac{\pi}{3}, \frac{\pi}{2}, \frac{2\pi}{3}\}$  and  $\varphi \in \{-\frac{3\pi}{4}, -\frac{\pi}{2}, -\frac{\pi}{4}, 0, \frac{\pi}{4}, \frac{\pi}{2}, \frac{3\pi}{4}, \pi\}$ . We then used  $f_\theta$  to find the corresponding actuator positions (i.e., blue dots in Figure 5). The final layout indicated that actuators should be positioned on body surface with greater curvatures (e.g., shoulders, waist) for optimal coverage of potential obstacle directions (**R1**). Directions with  $\vartheta = \frac{5\pi}{6}$  were omitted from the final layout because they did not align with upper body vibrations perceived by participants.

In our collision avoidance algorithm MultiCBF, this optimized layout was represented by a set of 32 actuators  $\mathcal{A} = \{\mathcal{A}_i\}_{i=1}^{32}$  and the corresponding directions set  $\hat{r}$  where  $\hat{r}_i$  represented the direction associated with actuator  $\mathcal{A}_i$ .

#### V. COLLISION AVOIDANCE ALGORITHM

In prior work, collision avoidance algorithms such as PRF [34] and CBF [4] only considered single-directional feedback due to the limited bandwidth of haptic joysticks. Since AeroHaptix was designed to support multi-point vibrations (**R3**), we extended CBF [4] to build a customized multi-directional feedback algorithm, **MultiCBF**:

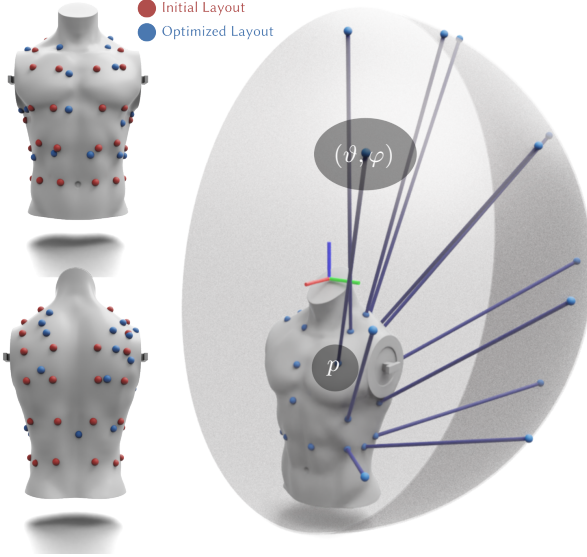


Fig. 5: The vibrotactile actuator layout, where the red dots depict the initial uniform distribution layout used in the perception study and the blue dots depict the final optimized layout. The lines illustrate the mappings between the perceived directions and body positions on the left side of the body.

1) Consider that the continuous-time dynamics of a UAV can be modelled with a double integrator, where the control input  $u$  corresponds to the acceleration command of the UAV. Let  $x = [q \ \dot{q}]^T$  with  $q$  and  $\dot{q}$  being the position and the velocity of the UAV respectively. The dynamics of the system then become

$$\dot{x} = \begin{bmatrix} \dot{q} \\ \ddot{q} \end{bmatrix} = f(x) + g(x)u, \quad (2)$$

where  $x \in \mathcal{X} \subset \mathbb{R}^n$ ,  $u \in \mathcal{U} \subset \mathbb{R}^m$ ,  $f : \mathcal{X} \rightarrow \mathbb{R}^n$  and  $g : \mathcal{X} \rightarrow \mathbb{R}^{n \times m}$  are Lipschitz continuous functions.

2) Consider a space with a set of obstacles  $\mathcal{B} = \{b_i\}_{i=1}^{|\mathcal{B}|}$ , where every obstacle  $b_i$  is associated with the center of mass  $q_{b_i}$ . For each obstacle  $b_i$ , we construct a set of safety constraints  $\mathcal{C}_i \in \mathcal{X}$  defined as

$$\mathcal{C}_i := \{x \in \mathcal{X} : h_i(x) \geq 0\}, \quad (3)$$

where  $h_i : \mathcal{X} \rightarrow \mathbb{R}$  is a continuously differentiable function that defines the safety boundary of obstacle  $b_i$ ,  $h_i(x) = 0 \Leftrightarrow x \in \partial\mathcal{C}_i$ .

3) We define the CBF  $\mathcal{U}_{\text{CBF}}$  for second-order systems as the set of all control inputs that keep the systems in the safe set  $\mathcal{C}$ . For the CBF associated with  $C_i$

$$\mathcal{U}_{\text{CBF},i}(h_i(x)) = \{u \in \mathcal{U} : L_f^2 h_i(x) + L_g L_f h_i(x)u + K[h_i(x) \ L_f h_i(x)]^T\} \geq 0, \quad (4)$$

where  $L_f h_i(x) = \nabla h_i(x)^T f(x)$ ,  $L_g h_i(x) = \nabla h_i(x)^T g(x)$  are the Lie derivatives of  $h_i(x)$ ,  $L_f^2 h_i(x)$  is the second-order Lie derivative of  $h_i(x)$ , and  $K$  is a positive constant that adjusts the safety margin.

4) Given user input  $u_{\text{ref}} \in \mathcal{U}$ , the optimization of a safe input  $u_{\text{safe},i}$  for obstacle  $b_i$  and its  $h_i(x)$  can be formulated as a quadratic program to find a **local safe input**  $u_{\text{safe},i} \in$

$\mathcal{U}_{\text{CBF},i}$  (Eq. 4) that is closest to  $u_{\text{ref}}$

$$u_{\text{safe},i} = \arg \min_{u \in \mathcal{U}} \frac{1}{2} \|u - u_{\text{ref}}\|^2 \text{ s.t. } u \in \mathcal{U}_{\text{CBF},i}(h_i(x)). \quad (5)$$

If  $u_{\text{safe},i} \neq u_{\text{ref}}$ , it means the user input  $u_{\text{ref}}$  violates the safety constraint  $C_i$ , then an actuator  $\mathcal{A}_j$  is triggered to notify the user. The choice of actuator  $\mathcal{A}_j$  is determined by the most aligned actuator direction  $\hat{r}_k$

$$j = \arg \max_{k \in 1:32} \left( \frac{q_{b_i} - q}{\|q_{b_i} - q\|} \cdot \hat{r}_k \right). \quad (6)$$

The vibration intensity  $I_j$  of actuator  $\mathcal{A}_j$  is then determined by the difference between the user input  $u_{\text{ref}}$  and the safe input  $u_{\text{safe},i}$  multiplied with a gain factor  $K_v$

$$I_j = \|K_v(u_{\text{safe},i} - u_{\text{ref}})\|. \quad (7)$$

Previous CBFs only considered a global safe input  $u_{\text{safe}}$  computed from a global safety set  $h(x) = \{h_i(x)\}_{i=1}^{|\mathcal{B}|}$  [4]. While this global safe input helped operators avoid obstacles, it was not sufficient to represent multiple obstacles and thus hindered operator's situational awareness. In contrast, MultiCBF computed local safe input for each obstacle and rendered haptic feedback independently.

## VI. SYSTEM EVALUATION

To evaluate AeroHaptix's ability to assist UAV teleoperation, we designed a study in which participants maneuvered a simulated UAV through cluttered tunnels. Twelve participants were recruited from our university campus to participate in the study (11 male, 1 female; mean age = 24 years, std = 3 years). Seven participants had previous experience operating UAVs. Each experiment lasted 70 minutes and each participant received \$40 CAD as compensation. The study was approved by our university's Research Ethics Board.

### A. Experimental Conditions

Participants experienced three **feedback conditions**: no feedback (NA), force shared control (FSC), and vibrotactile shared control (VSC). For the NA and VSC conditions, participants used an Xbox controller for input, which had a control mechanism similar to an RC controller. The output device was AeroHaptix with vibrotactile feedback rendered using MultiCBF. For the FSC condition, a Novint Falcon haptic joystick [5] was used for both input and output, similar to previous studies [35], [36]. Force feedback during FSC was rendered using CBF [4]. We hypothesized that VSC would enhance collision avoidance and input safety compared to NA, and reduce workload and increase sense of control compared to FSC.

Because previous studies often used complex experiment environments with varying visual capacities [3], [9], [17], it was unclear when haptic feedback was beneficial. In this study, we used three **flying directions** to assess how visual capacity influenced participants' reliance on haptic feedback: forward (FWD), right (R) and upward (UP). In the forward direction, participants received substantial visual information about upcoming obstacles because the UAV was oriented to

face the flying direction. In contrast, visual capacity in other directions were limited, and this may increase the difficulty for collision avoidance. Due to the MultiCBF algorithm, we also hypothesized that VSC would outperform FSC in delivering obstacle information.

Our hypotheses were that:

- (H<sub>1</sub>) compared to NA, VSC would reduce the number of collisions and input disagreement
- (H<sub>2</sub>) compared to flying forward, the number of collisions would be higher when flying right and upward
- (H<sub>3</sub>) compared to FSC, VSC would reduce task workload
- (H<sub>4</sub>) compared to FSC, VSC would increase participants' sense of control
- (H<sub>5</sub>) compared to FSC, VSC would be more effective at increasing situational awareness

### B. Experimental Setup

The study was performed in a simulated UAV environment that was built using Microsoft AirSim [37]. During the study, participants operated a simulated quadrotor with a front-facing camera. The simulation was run on an Alienware M15 Laptop with RTX 3060 Ti GPU.

The experimental scene was a  $5 \times 5 \times 50$ m tunnel (Figure 6) that could face forward, right, or upward depending on the flying directions. The scene contained four planes and fifteen obstacles that were of three types, i.e., cubes, spheres, and cylinders. The safety boundary of plane  $b_i$  was defined as:  $h_i(x) = h_i([q \quad \dot{q}]^T) = (q - q_{b_i}) \times \hat{n}_{b_i}$ , where  $q_{b_i}$  was the center of mass and  $\hat{n}_{b_i}$  was the unit normal of plane  $b_i$ . The safety boundaries of other obstacles were approximated using super-ellipsoids  $h_i(x) = h([q \quad \dot{q}]^T) = \left(\frac{q_1 - q_{b_i,1}}{a_1}\right)^n + \left(\frac{q_2 - q_{b_i,2}}{a_2}\right)^n + \left(\frac{q_3 - q_{b_i,3}}{a_3}\right)^n$ , where  $q_{b_i}$  was the center of mass and  $a$  was the scaling vector of obstacle  $b_i$ . Obstacle positions were randomized to avoid learning effects.



Fig. 6: The first-person view of the simulation environment used in the study, with randomly positioned obstacles. A top-down overview is on the right.

On each simulation frame, the system detected input commands from the controller, received UAV state updates from AirSim, and checked if safety constraints were violated using collision avoidance algorithms. If haptic feedback was enabled, then the system would send vibration or force feedback commands to the corresponding output device. At the end of each frame, the system updated the UAV's state in AirSim.

At the beginning of the study, the participant reviewed and signed a consent form. Then, the participant was briefed on the study purpose and overall procedure. Following this, the participant experienced the three feedback conditions in a randomized order ( $3 \times 3$  Latin square). For each feedback condition, the participant underwent a practice round with designated devices for five minutes. Then, the participant operated the UAV to fly through three tunnels, one for each flying direction. After each condition, the participant completed a questionnaire about task workload and their sense of control.

### C. Metrics and Analysis

We collected both objective and subjective measurements. Objective measurements included the total distance travelled, number of collisions, and input disagreement (computed as the difference between participant input and safe input  $\|u_{\text{ref}} - u_{\text{safe}}\|$ ), which evaluated the collision avoidance performance (H<sub>1</sub>, H<sub>2</sub>). For each metric, we conducted a two-way repeated measures ANOVA using SPSS. If significant effects were found, post-hoc pairwise comparisons using a Bonferroni correction were conducted.

Subjective measurements included NASA-TLX [38] questions that evaluated task load (H<sub>3</sub>), and four 7-point Likert questions adapted from previous work [8] that probed sense of control (H<sub>4</sub>):

- 1) How easy was it to control drone with this input device?
- 2) How much control did you feel you had over the drone?
- 3) How well did the drone's motion match your intention?
- 4) If you felt haptic feedback, how much did the feedback help you navigate the robot?

For each metric, we conducted a Friedman test. If significant effects were found, post-hoc pairwise comparisons using Wilcoxon signed-rank tests were conducted.

To evaluate situational awareness (H<sub>5</sub>), a pop-up window appeared at a random time during the flight for each direction (with the simulation paused) and participants were asked to report any perceived obstacles. This technique was adapted from situational awareness probing techniques like SAGAT and SPAM [39]. Reported obstacles were categorized into *visual obstacles* that were visible at pause, and *haptic obstacles* that were not seen but perceived through haptic feedback. Since the visual capacity is consistent across conditions, haptic obstacles represent the enhanced situational awareness through haptic feedback. A two-way repeated measures ANOVA is run to determine the effect of haptic feedback conditions and flying directions on situational awareness.

### D. Results

1) *Objective Measurements*: For total distance travelled, the RM-ANOVA determined that feedback condition had a significant effect ( $F(2, 22) = 3.585, p < 0.05$ ), as did flying direction ( $F(2, 22) = 17.868, p < 0.001$ ). The interaction between feedback condition and flying direction was also significant ( $F(1.957, 21.527) = 4.916, p < 0.01$ ). The post-hoc analysis of the interaction effect revealed that FSC-R had a significantly longer distance than FSC-FWD ( $p < 0.01$ ),

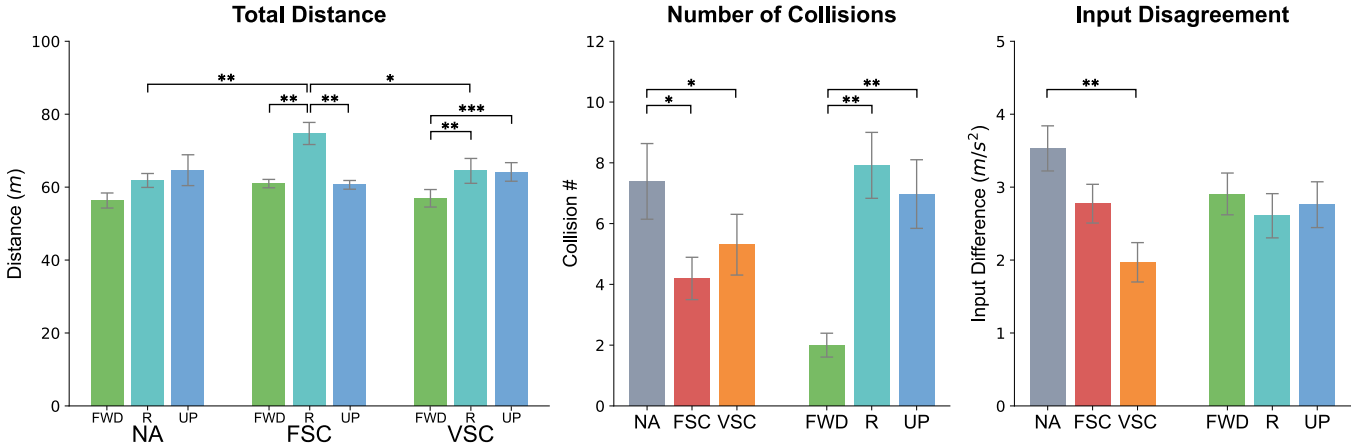


Fig. 7: Objective measurement results grouped by feedback condition (NA - no feedback, FSC - force shared control, VSC - vibrotactile shared control) and flying direction (FWD - forward, R - right, UP - upward). The error bars represent the standard error of the mean (SEM), \* $p < 0.05$ , \*\* $p < 0.01$ , and \*\*\* $p < 0.001$ .

FSC-UP ( $p < 0.01$ ), NA-R ( $p < 0.01$ ), and VSC-R ( $p < 0.05$ ), while VSC-FWD had a significantly shorter distance than VSC-R ( $p < 0.01$ ) and VSC-UP ( $p < 0.001$ ).

For the number of collisions, the RM-ANOVA determined that feedback condition had a significant effect ( $F(2, 22) = 8.095, p < 0.01$ ), as did flying direction ( $F(2, 22) = 15.653, p < 0.001$ ). No interaction was found between feedback condition and flying direction ( $F(2.168, 23.846) = 1.910, p = 0.168$ ). Post-hoc pairwise comparisons revealed that NA caused more collisions than FSC ( $p < 0.05$ ) and VSC ( $p < 0.05$ ) and that flying forward caused fewer collisions than right ( $p < 0.01$ ) and upward ( $p < 0.01$ ).

For input disagreement, the RM-ANOVA determined that feedback condition had a significant effect ( $F(2, 22) = 4.798, p < 0.05$ ), while flying direction did not ( $F(1.254, 13.789) = 0.628, p = 0.476$ ). The interaction between feedback condition and flying direction was also not significant ( $F(4, 44) = 1.566, p = 0.200$ ). Post-hoc pairwise comparisons revealed that there was less disagreement with VSC than NA ( $p < 0.01$ ).

In summary, VSC caused fewer collisions and less input disagreement than NA. Additionally, the right and upward directions caused more collisions than the forward direction, highlighting the impact of reduced visual capacity when the camera was not aligned with the flying direction. Thus, **H1** and **H2** were accepted.

2) *Subjective Measurements*: physical demand: NA ; FSC, effort: NA ; FSC,

Friedman tests determined that feedback condition had a significant effects on physical demand ( $\chi^2(2) = 12.950, p < 0.01$ ), effort ( $\chi^2(2) = 7.294, p < 0.05$ ), overall task load ( $\chi^2(2) = 6.048, p < 0.05$ ), Q3 Matching Intention ( $\chi^2(2) = 7.056, p < 0.05$ ), and Q4 Haptic Usefulness ( $\chi^2(2) = 21.378, p < 0.001$ ). Post-hoc pairwise comparisons revealed that NA required less physical demand than FSC ( $p < 0.01$ ), VSC required less effort than FSC ( $p < 0.05$ ), and VSC was more helpful than FSC ( $p < 0.05$ ). Since significant differences were only found for some metrics, **H3** and **H4** were not accepted.

3) *Situational Awareness*: The numbers of reported haptic obstacles are reported in Figure 8. the RM-ANOVA determined that feedback condition had a significant effect ( $F(1, 11) = 7.436, p < 0.05$ ), while flying direction did not ( $F(2, 22) = 2.131, p = 0.143$ ). The interaction between feedback condition and flying direction was also not significant ( $F(2, 22) = 0.517, p = 0.604$ ). Post-hoc pairwise comparisons revealed that VSC was more effective at enhancing situational awareness than FSC ( $p < 0.05$ ). Therefore, **H5** was accepted.

## VII. DISCUSSION

In this section, we discuss the design implications arising from the experiment results.

### A. Benefits of Vibrotactile Feedback

Vibrotactile feedback resolved the direct coupling problem with haptic joystick systems and ensured stable operation. When using FSC, operators struggled to understand the intent of the force feedback and often tried to override the input with manual force in the opposite direction. This inevitably resulted in risky and oscillatory movements in the tunnel, which was further confirmed by the longer flying distances and higher input disagreement. When using VSC, however, the decoupling of the input and output channels via the RC controller and AeroHaptix provided operators with full control over their UAV. Operators had sufficient time to process the vibrotactile cues and then steer the UAV towards a safe trajectory. Thus, VSC promoted safer and more cautious operation, reducing the risk of collisions in real world scenarios.

Additionally, vibrotactile feedback enhanced situational awareness by delivering multi-directional cues through the MultiCBF algorithm. More obstacles were identified through haptic feedback when using VSC than FSC. This indicated that operators could effectively understand vibrotactile feedback and became more aware of the environment.

We acknowledged that the subjective assessment of VSC, task workload and sense of control, showed no statistical

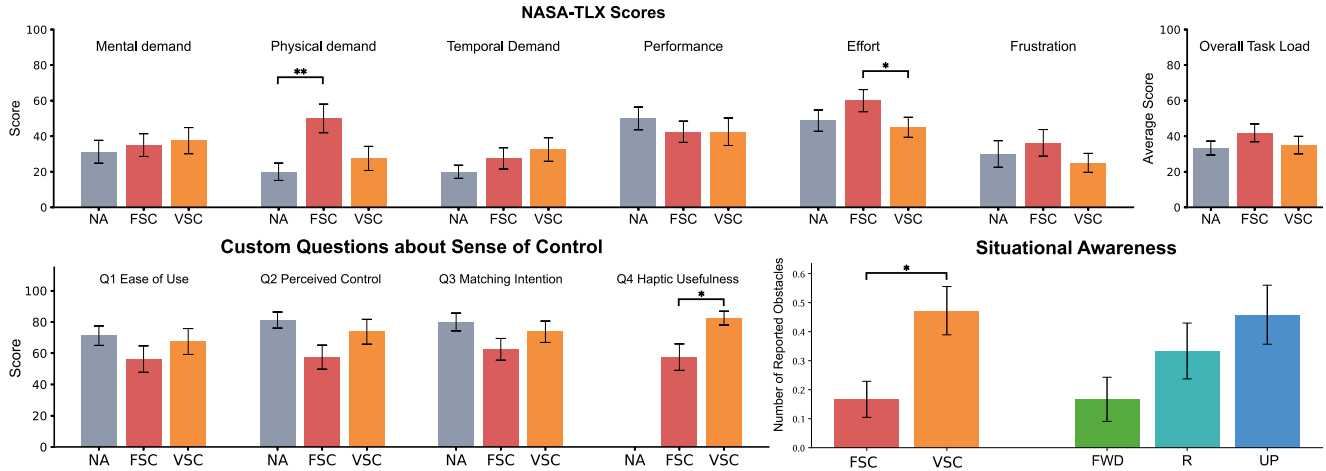


Fig. 8: The subjective measurements and situational awareness results grouped by feedback condition (NA - no feedback, FSC - force shared control, VSC - vibrotactile shared control) and flying direction (FWD - forward, R - right, UP - upward). The error bars represent the standard error of the mean (SEM),  $*p < 0.05$ ,  $**p < 0.01$ , and  $***p < 0.001$ .

difference from FSC. This was likely due to the short duration of the experimental tasks, which lasted approximately 1 minute per flight. This prevented participants from experiencing the types of workloads typically associated with longer real-world teleoperation. Future research should consider extending the task duration to gain a deeper understanding of the differences between the two.

#### B. Effect of Visual Capacity

The isolated flying directions helped assess how visual capacity influenced operator's reliance on haptic feedback. When obstacles were out of sight in right and upward directions, the numbers of collisions were three times more than the forward direction. This suggested that haptic feedback was more helpful in low visual capacity conditions. Due to the limited obstacles in the tunnels, no statistical difference was found across flying directions on situational awareness. Future research can increase obstacles to highlight the effectiveness of haptic feedback in low visibility scenarios.

Besides flying directions, factors such as light sources and dust [40] can also impair visual capacity in real-world scenarios. Future research could investigate these factors and refine algorithms to dynamically adjust haptic feedback.

#### C. Intuitive Mappings from Layout Optimization

Our layout optimization process eliminated perceptual biases and ensured an intuitive mapping between body positions and obstacle directions, which helped reduce perceived workloads during teleoperation with vibrotactile assistance. As no significant differences were found between the NA and VSC conditions, the addition of vibrotactile feedback on the body likely did not impose extra processing workload.

On the contrary, FSC caused significantly higher physical demand than NA and required more effort than VSC. This indicates that the removal of the RC controller and the direct coupling of input and output channels imposed control challenges that could be attributed to force feedback misalignment. Previous approaches that rendered force feedback often

overlooked the anisotropy of force perception and magnitude on the hand [32], [33], leading to perceptual differences in force feedback from various directions. These findings thus reinforce the importance of addressing perceptual biases in future haptic device design for UAV teleoperation.

#### VIII. LIMITATIONS AND FUTURE WORK

Although the results showed that on-body vibrotactile feedback was effective at enhancing collision avoidance during UAV teleoperation, there are a few limitations. First, as discussed in Section IV-C, upper-body vibrations are limited in representing obstacles below the drone. Currently, we had to map them to the lower back actuators. In the future, We plan to extend vibrotactile feedback to the upper limbs or lower body to alleviate this problem.

Second, UAV teleoperation was simulated in a simplified virtual environment, without considering real-world factors such as communication delays, inaccurate UAV state estimations, or control input constraints, as outlined by Lam et al. [34]. To understand the role of such factors, we plan to integrate AeroHaptix into commercial UAVs using developer tools such as DJI SDKs.

Third, we only modulated the actuator positions and vibration intensities to convey obstacle directions. Future work could utilize more vibration parameters to enrich the information provided about obstacles, such as obstacle types and mobility. As prior research has suggested, the use of frequency, spatial, and temporal patterns could also be viable when rendering such information [19].

#### IX. CONCLUSION

This work introduced AeroHaptix, a novel vibrotactile feedback system for collision avoidance during UAV teleoperation. The system was built using custom hardware that featured high-density actuators, fine-grained control, and low-latency communication. An optimal actuator layout was derived from a perceptual study to ensure obstacle directions could be uniformly conveyed across the upper body. Using

a novel multi-point feedback algorithm (i.e., MultiCBF), AeroHaptix was found to enhance collision avoidance and reduce input disagreement, without inducing extra workload. We encourage future researchers to build on our work to innovate haptic feedback devices to assist operators with UAV teleoperation.

## REFERENCES

- [1] T. M. Lam, H. W. Boschloo, M. Mulder, and M. M. Van Paassen, “Artificial force field for haptic feedback in uav teleoperation,” *IEEE Trans. on Syst., Man, and Cybern.-Part A: Syst. and Humans*, vol. 39, no. 6, pp. 1316–1330, 2009.
- [2] A. M. Brandt and M. B. Colton, “Haptic collision avoidance for a remotely operated quadrotor uav in indoor environments,” in *2010 IEEE Int. Conf. on Syst., Man and Cybern.* IEEE, 2010, pp. 2724–2731.
- [3] X. Hou and R. Mahony, “Dynamic kinesthetic boundary for haptic teleoperation of vtol aerial robots in complex environments,” *IEEE Trans. on Syst., Man and Cybern.: Syst.*, vol. 46, no. 5, pp. 694–705, 2015.
- [4] D. Zhang, G. Yang, and R. P. Khurshid, “Haptic teleoperation of uavs through control barrier functions,” *IEEE Trans. on Haptics*, vol. 13, no. 1, pp. 109–115, 2020.
- [5] N. T. Inc, “Novint falcon,” <https://hapticshouse.com/pages/novints-falcon-haptic-device>, 2024, accessed: Feb 24, 2024.
- [6] D. Syst., “Touch haptic device,” <https://www.3dsystems.com/haptics-devices/touch>, 2024, accessed: Feb 24, 2024.
- [7] F. Dimension, “Force dimension - haptic devices,” <https://www.forcedimension.com/products>, 2024, accessed: Feb 24, 2024.
- [8] D. Zhang, R. Tron, and R. P. Khurshid, “Haptic feedback improves human-robot agreement and user satisfaction in shared-autonomy teleoperation,” in *2021 IEEE Int. Conf. on Robot. and Automat. (ICRA)*. IEEE, 2021, pp. 3306–3312.
- [9] R. M. Philbrick and M. B. Colton, “Effects of haptic and 3d audio feedback on operator performance and workload for quadrotor uavs in indoor environments,” *J. of Robotics and Mechatronics*, vol. 26, no. 5, pp. 580–591, 2014.
- [10] A. M. Brandt, “Haptic collision avoidance for a remotely operated quadrotor uav in indoor environments,” 2009.
- [11] V. Ho, C. Borst, M. M. van Paassen, and M. Mulder, “Increasing acceptance of haptic feedback in uav teleoperation by visualizing force fields,” in *2018 IEEE Int. Conf. on Syst., Man, and Cybern. (SMC)*. IEEE, 2018, pp. 3027–3032.
- [12] C. Rognon, A. R. Wu, S. Mintchev, A. Ijspeert, and D. Floreano, “Haptic guidance with a soft exoskeleton reduces error in drone teleoperation,” in *Haptics: Science, Technology, and Applications: 11th International Conference, EuroHaptics 2018, Pisa, Italy, June 13–16, 2018, Proceedings, Part II 11*. Springer, 2018, pp. 404–415.
- [13] C. Rognon, V. Ramachandran, A. R. Wu, A. J. Ijspeert, and D. Floreano, “Haptic feedback perception and learning with cable-driven guidance in exosuit teleoperation of a simulated drone,” *IEEE transactions on haptics*, vol. 12, no. 3, pp. 375–385, 2019.
- [14] S.-G. Hong, B. S. Kim, S. Kim, and J.-J. Lee, “Artificial force reflection control for teleoperated mobile robots,” *Mechatronics*, vol. 8, no. 6, pp. 707–717, 1998.
- [15] H. W. Boschloo, T. M. Lam, M. Mulder, and M. Van Paassen, “Collision avoidance for a remotely-operated helicopter using haptic feedback,” in *2004 IEEE Int. Conf. on Syst., Man and Cybern.*, vol. 1. IEEE, 2004, pp. 229–235.
- [16] X. Hou and R. Mahony, “Dynamic kinesthetic boundary for haptic teleoperation of aerial robotic vehicles,” in *2013 IEEE/RSJ Int. Conf. on Intell. Robots and Syst.* IEEE, 2013, pp. 4549–4950.
- [17] H. Courtois, N. Aouf, K. Ahiska, and M. Cecotti, “Oast: Obstacle avoidance system for teleoperation of uavs,” *IEEE Trans. on Human-Machine Syst.*, vol. 52, no. 2, pp. 157–168, 2022.
- [18] C. Louison, F. Ferlay, and D. R. Mestre, “Spatialized vibrotactile feedback contributes to goal-directed movements in cluttered virtual environments,” in *2017 IEEE Symp. on 3D User Interfaces (3DUI)*. IEEE, 2017, pp. 99–102.
- [19] V. A. de Jesus Oliveira, L. Brayda, L. Nedel, and A. Maciel, “Designing a vibrotactile head-mounted display for spatial awareness in 3d spaces,” *IEEE Trans. on Vis. and Comp. Graph.*, vol. 23, no. 4, pp. 1409–1417, 2017.
- [20] J. Y. F. Lee, N. Rajeev, and A. Bhojan, “Goldeye: Enhanced spatial awareness for the visually impaired using mixed reality and vibrotactile feedback,” in *ACM Multimedia Asia*, 2021, pp. 1–7.
- [21] G. Flores, S. Kurniawan, R. Manduchi, E. Martinson, L. M. Morales, and E. A. Sisbot, “Vibrotactile guidance for wayfinding of blind walkers,” *IEEE Trans. on Haptics*, vol. 8, no. 3, pp. 306–317, 2015.
- [22] H.-C. Wang, R. K. Katschmann, S. Teng, B. Araki, L. Giarré, and D. Rus, “Enabling independent navigation for visually impaired people through a wearable vision-based feedback system,” in *2017 IEEE Int. Conf. on Robotics and Automat. (ICRA)*. IEEE, 2017, pp. 6533–6540.
- [23] M. A. B. Mohammed Zaffir and T. Wada, “Presentation of robot-intended handover position using vibrotactile interface during robot-to-human handover task,” in *Proc. of the 2024 ACM/IEEE Int. Conf. on Human-Robot Interact.*, 2024, pp. 492–500.
- [24] S. Grushko, A. Vysocky, D. Heczko, and Z. Bobovský, “Intuitive spatial tactile feedback for better awareness about robot trajectory during human–robot collaboration,” *Sensors*, vol. 21, no. 17, p. 5748, 2021.
- [25] P. Xia, K. McSweeney, F. Wen, Z. Song, M. Krieg, S. Li, X. Yu, K. Crippen, J. Adams, and E. J. Du, “Virtual telepresence for the future of rov teleoperations: opportunities and challenges,” in *SNAME Offshore Symp.* SNAME, 2022, p. D011S001R001.
- [26] P. G. De Barros, R. W. Lindeman, and M. O. Ward, “Enhancing robot teleoperator situation awareness and performance using vibro-tactile and graphical feedback,” in *2011 IEEE Symp. on 3D User Interfaces (3DUI)*. IEEE, 2011, pp. 47–54.
- [27] D. Wittchen, K. Spiel, B. Fruchard, D. Degraen, O. Schneider, G. Freitag, and P. Strohmeier, “Tactjam: An end-to-end prototyping suite for collaborative design of on-body vibrotactile feedback,” in *16th Int. Conf. on Tangible, Embedded, and Embodied Interact.*, 2022, pp. 1–13.
- [28] A. Dementev, P. Getreuer, D. Kanevsky, M. Slaney, and R. F. Lyon, “Vhp: vibrotactile haptics platform for on-body applications,” in *The 34th Annu. ACM Symp. on User Interface Softw. and Technol.*, 2021, pp. 598–612.
- [29] bHaptics, “bhaptics: Tactile feedback for vr, gaming, and music,” 2023. [Online]. Available: <https://www.bhaptics.com/>
- [30] J. B. Van Erp, “Presenting directions with a vibrotactile torso display,” *Ergonomics*, vol. 48, no. 3, pp. 302–313, 2005.
- [31] H. Elsayed, M. Weigel, F. Müller, M. Schmitz, K. Marky, S. Günther, J. Riemann, and M. Mühlhäuser, “Vibromap: Understanding the spacing of vibrotactile actuators across the body,” *Proceedings of the ACM on Interactive, Mobile, Wearable and Ubiquitous Technologies*, vol. 4, no. 4, pp. 1–16, 2020.
- [32] F. E. Van Beek, W. M. B. Tiest, and A. M. Kappers, “Anisotropy in the haptic perception of force direction and magnitude,” *IEEE Trans. on Haptics*, vol. 6, no. 4, pp. 399–407, 2013.
- [33] H. Z. Tan, F. Barbagli, J. Salisbury, C. Ho, and C. Spence, “Force-direction discrimination is not influenced by reference force direction (short paper),” 2006.
- [34] T. M. Lam, M. Mulder, and M. Van Paassen, “Collision avoidance in uav tele-operation with time delay,” in *2007 IEEE Int. Conf. on Syst., Man and Cybern.* IEEE, 2007, pp. 997–1002.
- [35] S. Omari, M.-D. Hua, G. Ducard, and T. Hamel, “Bilateral haptic teleoperation of vtol uavs,” in *2013 IEEE Int. Conf. on Robot. and Automat.* IEEE, 2013, pp. 2393–2399.
- [36] S. Reyes, H. Romero, S. Salazar, R. Lozano, and O. Santos, “Outdoor haptic teleoperation of a hexarotor uav,” in *2015 Int. Conf. on Unmanned Aircr. Syst. (ICUAS)*. IEEE, 2015, pp. 972–979.
- [37] S. Shah, D. Dey, C. Lovett, and A. Kapoor, “Airsim: High-fidelity visual and physical simulation for autonomous vehicles,” in *Field and Service Robot.*, 2017. [Online]. Available: <https://arxiv.org/abs/1705.05065>
- [38] S. G. Hart and L. E. Staveland, “Development of nasa-tlx (task load index): Results of empirical and theoretical research,” in *Advances in psychology*. Elsevier, 1988, vol. 52, pp. 139–183.
- [39] M. R. Endsley, “A systematic review and meta-analysis of direct objective measures of situation awareness: a comparison of sagat and spam,” *Human factors*, vol. 63, no. 1, pp. 124–150, 2021.
- [40] T.-C. Hung, Y.-R. Li, and C.-C. Peng, “Uav inspection in heavy industry: Preliminary trial and challenge,” in *2024 International Conference on Consumer Electronics-Taiwan (ICCE-Taiwan)*. IEEE, 2024, pp. 135–136.